First Constraints on the Photon Coupling of Axionlike Particles from Multimessenger Studies of the Neutron Star Merger GW170817

P. S. Bhupal Dev[1,*] Jean-François Fortin,[2,†] Steven P. Harris[3,‡] Kuver Sinha,[4,§] and Yongchao Zhang[5,‖]

[1]*Department of Physics and McDonnell Center for the Space Sciences, Washington University, St. Louis, Missouri 63130, USA*
[2]*Département de Physique, de Génie Physique et d'Optique, Université Laval, Québec, Quebec G1V 0A6, Canada*
[3]*Institute for Nuclear Theory, University of Washington, Seattle, Washington 98195, USA*
[4]*Department of Physics and Astronomy, University of Oklahoma, Norman, Oklahoma 73019, USA*
[5]*School of Physics, Southeast University, Nanjing 211189, China*

We use multimessenger observations of the neutron star merger event GW170817 to derive new constraints on axionlike particles (ALPs) coupling to photons. ALPs are produced via Primakoff and photon coalescence processes in the merger, escape the remnant, and decay back into two photons, giving rise to a photon signal approximately along the line of sight to the merger. We analyze the spectral and temporal information of the ALP-induced photon signal and use the *Fermi* Large Area Telescope (Fermi-LAT) observations of GW170817 to derive our new ALP constraints. We also show the improved prospects with future MeV γ-ray missions, taking the spectral and temporal coverage of Fermi-LAT as an example.

Introduction.—The extreme astrophysical environments in the vicinity of black holes (BHs), neutron stars (NSs), magnetars, and binary BH and NS mergers have recently emerged as a new tool for probing light dark-sector physics, complementary to and beyond the traditional arena of stellar and supernova environments [1]. Much of this recent progress is driven by data from across the electromagnetic spectrum, as well as neutrinos and gravitational waves (GWs), together with the exciting prospects of multimessenger studies [2,3]. In particular, the discovery of the NS merger event GW170817 [4] has opened a new window to beyond-the-standard-model (BSM) particle searches, such as axions and axionlike particles (ALPs) [5–11], *CP*-even scalars [12], and dark photons [13]. The purpose of this Letter is to utilize the multimessenger studies of GW170817 [4,14,15] to derive new constraints on ALPs.

Our main idea is depicted in Fig. 1. A generic feature of the QCD axion [16–21], or any pseudoscalar ALP [22,23], is its coupling to photons $g_{a\gamma\gamma}$, which is central to most of the ALP searches [24,25]. The relevant Lagrangian is

$$\mathcal{L} \supset \frac{1}{2}\partial^\mu a \partial_\mu a - \frac{1}{2}m_a^2 a^2 - \frac{1}{4}g_{a\gamma\gamma}aF^{\mu\nu}\tilde{F}_{\mu\nu}, \qquad (1)$$

where a is the ALP field, m_a is its mass, $F^{\mu\nu}$ is the electromagnetic field strength tensor, and $\tilde{F}_{\mu\nu}$ is its dual. ALPs can then be produced via the Primakoff and photon

coalescence processes in the NS merger. Depending on their mass and coupling, they could escape the merger environment and subsequently decay into two photons. This ALP-induced photon spectrum, which mostly falls in the (soft) γ-ray or (hard) x-ray regime, is compared to the flux *upper* limits obtained by x- and γ-ray observations of GW170817 for various energy ranges and time intervals
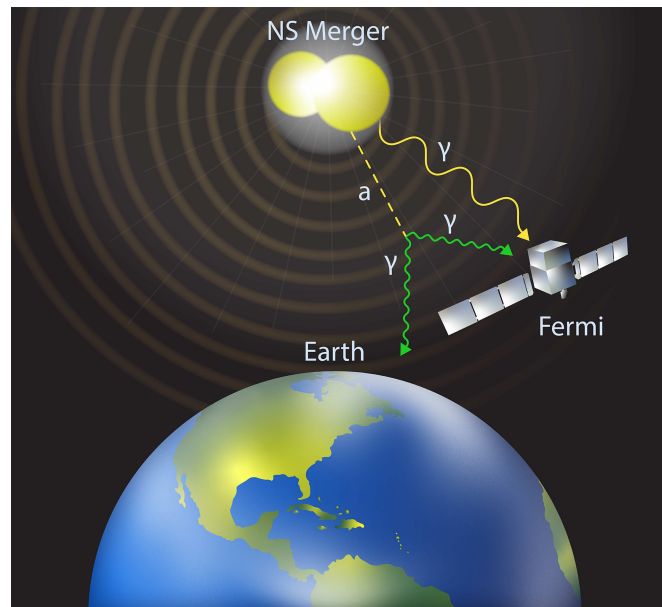

FIG. 1. An artist's rendition of our main idea. The ALP (dashed line), after being produced in the NS merger, escapes and decays outside the merger environment into photons, which can be detected by the *Fermi* satellite (or future MeV γ-ray telescopes).

relative to the GW signal [15,26–29] to derive the first merger constraints in the $(m_a, g_{a\gamma\gamma})$ parameter space.

ALP production.—The hot, dense matter in a NS merger remnant would efficiently produce ALPs coupling to photons. The two main production mechanisms are the Primakoff process $\gamma + p \to a + p$ (p being a proton), where electromagnetic scattering essentially converts a photon into an ALP, and photon coalescence $\gamma + \gamma \to a$. These processes occur in medium, where the properties of the photon are modified due to the high densities [1]. The photon picks up a longitudinal mode (though we will neglect this degree of freedom in this Letter), and the two conventional transverse modes are altered—in essence, the photon picks up a mass m_γ, which is equal to the plasma frequency $\omega_{\rm pl}$. Our Primakoff calculation includes the recoil of the charged particle, as well as the electromagnetic screening of the exchanged photon, while the photon coalescence calculation is computed in the usual manner. In both processes, we include the full distribution functions—Fermi-Dirac or Bose-Einstein. More details pertaining to electromagnetism in a dense medium and the local production rate calculations are presented in the Supplemental Material [30].

The production spectrum is then integrated over the entire merger remnant. We use one of the merger profiles calculated in Ref. [50] (available on Zenodo [51]), which use the ALF2 equation of state [52,53]. We include the gravitational gravitational redshift and trapping factor that prevents ALPs with sufficiently low kinetic energy from escaping the deep potential well of the merger remnant. In the region of parameter space that we study, the ALP mean free path in the merger remnant is long enough that ALP trapping due to inverse Primakoff or two-photon decay is negligible.

After the two NSs collided in GW170817, the resulting merger remnant [54] survived for about 1 sec before collapsing to a BH [55]. While ALPs would be produced in the (cold) constituent NSs before they merge, the production rate strongly increases with temperature [56]. When the two NSs merge, their temperature rises from keV [57] to tens of MeV [58]. Thus the ALP production rate from the binary NS system as a function of time will dramatically upsurge once the stars merge and heat up. We assume that the merger remnant produces ALPs at a constant rate for 1 sec, starting from the time of collision (heating occurs within a few milliseconds of this time) and ending when the remnant collapses to a BH. Since the merger profiles provided in Ref. [50] are time-independent configurations, we use the same profile for the entire lifetime of the remnant. We have checked that, in the
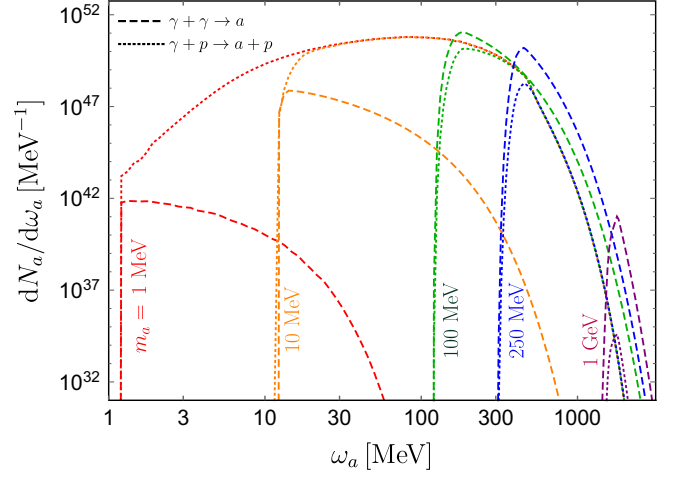

FIG. 2. ALP production spectrum from a merger remnant, assuming constant emission for 1 sec and for $g_{a\gamma\gamma} = 10^{-10}$ GeV^{-1}. Note the switchover between Primakoff and photon coalescence at $m_a \approx 100$ MeV.

parameter space we eventually constrain, the ALP emission does not substantially cool the remnant.

The time-integrated ALP production spectrum (as observed at infinity) is plotted in Fig. 2 for several different values of the ALP mass. The Primakoff and photon coalescence contributions are displayed separately. The ALP-photon coupling is set to $g_{a\gamma\gamma} = 10^{-10}$ GeV^{-1}, and gravitational redshift and trapping are included. Without gravitational trapping, the spectra would start at $\omega_a = m_a$, representing a zero kinetic energy ALP. However, such an ALP could not escape the potential well of the merger remnant and thus would not reach an observer at infinity. Gravitational trapping is much more severe for high-mass ALPs, for example, the $m_a = 1$ GeV case in this figure. The dominant production mechanism for low-mass ALPs is Primakoff and for high-mass ALPs is photon coalescence. The switchover occurs somewhere around $m_a \approx 100$ MeV. For low-mass ALPs, the production peaks around energies of 100 MeV, which is due to the temperature T of the environment in which they are produced. For ALPs with masses $m_a \gtrsim 3T$, the dominant contribution to their energy comes from their rest mass, so their spectrum peaks at energies just above their rest mass (which is why gravitational trapping so diminishes their spectrum).

Photon spectrum.—The photon flux F_γ observed at Earth is given by

$$\omega_\gamma^2 \frac{d^2 F_\gamma}{d\omega_\gamma dt}(\omega_\gamma, D + t) = \int_{-1}^{1} dz \int_0^\infty dL \frac{\omega_\gamma^2}{4\pi D(L_\gamma + Lz)} \frac{d^2 N_a}{d\omega_a dt}(\omega_a, D + t - L/\beta_a - L_\gamma) {\rm Jac}(\omega_a, \omega_\gamma)$$

$$\times \frac{m_a^2}{\omega_a^2(1 - \beta_a z)^2} \frac{\exp(-L/\ell_a)}{\ell_a} \Theta(L - R_\star)\Theta(L - D/\sqrt{1 - z^2}). \qquad (2)$$

The various parameters in Eq. (2) are the photon energy ω_γ, the Earth-merger distance D, the photon arrival time t compared to GW arrival time (with $t = 0$ being the arrival time of the GW), the ALP-to-photon decay angle $z = \cos\alpha$ in the ALP frame (see Fig. S6 of the Supplemental Material [30]), the distance L traveled by the ALP before decaying, the distance L_γ traveled by the photon before reaching the detector, the ALP spectrum N_a as a function of the ALP energy ω_a (cf. Fig. 2), the Jacobian $\text{Jac}(\omega_a, \omega_\gamma)$ of the transformation from ALP energy to photon energy, the ALP velocity β_a, the (boosted) ALP decay length ℓ_a, and the minimal distance $R_\star$ that ALPs must reach before decaying such that the emitted photons are unlikely to be absorbed by the ejecta in the outskirts of the remnant. The different contributions to Eq. (2) are explained in detail in the Supplemental Material [30]. We take benchmark values of $D = 40$ Mpc and $R_\star = 1000$ km for a GW170817-like NS merger (see Ref. [13]).

An important feature of Eq. (2) pertains to the temporal dependence of the photon signal, which is critical for multimessenger studies. Although the production of ALPs from the merger environment lasts for 1 sec and is taken to be time independent, the photon flux from ALP decay has a nontrivial time dependence, as shown in Fig. 3, coming from the decay geometry

(cf. Fig. S6 [30]). Two benchmarks (both currently unconstrained by other methods) for the ALP mass and coupling are chosen: benchmark 1 ($m_a = 398$ MeV, $g_{a\gamma\gamma} = 5.01 \times 10^{-11}$ GeV^{-1}) and benchmark 2 ($m_a = 200$ MeV, $g_{a\gamma\gamma} = 1.41 \times 10^{-12}$ GeV^{-1}), in the left and right panels of Fig. 3, respectively. The top (bottom) panels of Fig. 3 display the flux as a function of the arrival time t (photon energy ω_γ), and the contours of different colors correspond to spectral (temporal) snapshots of photon energy (arrival time). The time window corresponding to *Fermi* Large Area Telescope (Fermi-LAT) data [28] is shown by the vertical gray-shaded region in the top right panel.

Several observations are in order: (i) For ALPs that are longer-lived, corresponding to smaller values of $g_{a\gamma\gamma}$ and/or m_a (benchmark 2), the photon flux reaches a temporal plateau around $t \sim 1$ sec that persists up to $t \sim 10^4$ sec for the photon energies displayed (top right panel in Fig. 3). For this time span $t \sim (1–10^4)$ sec, the spectral peak lies at $\omega_\gamma \sim 300$ MeV corresponding to $\omega_\gamma^2 d^2 F_\gamma / d\omega_\gamma dt \sim 10^{-5}$ MeV/cm^2/sec (bottom right panel). At these early times, a γ-ray telescope that has its peak sensitivity around $\omega_\gamma \sim \mathcal{O}(300)$ MeV would be most suitable for multimessenger studies. The photon signal typically diminishes around $t \sim \mathcal{O}(10^5)$ sec, signifying the latest times that a
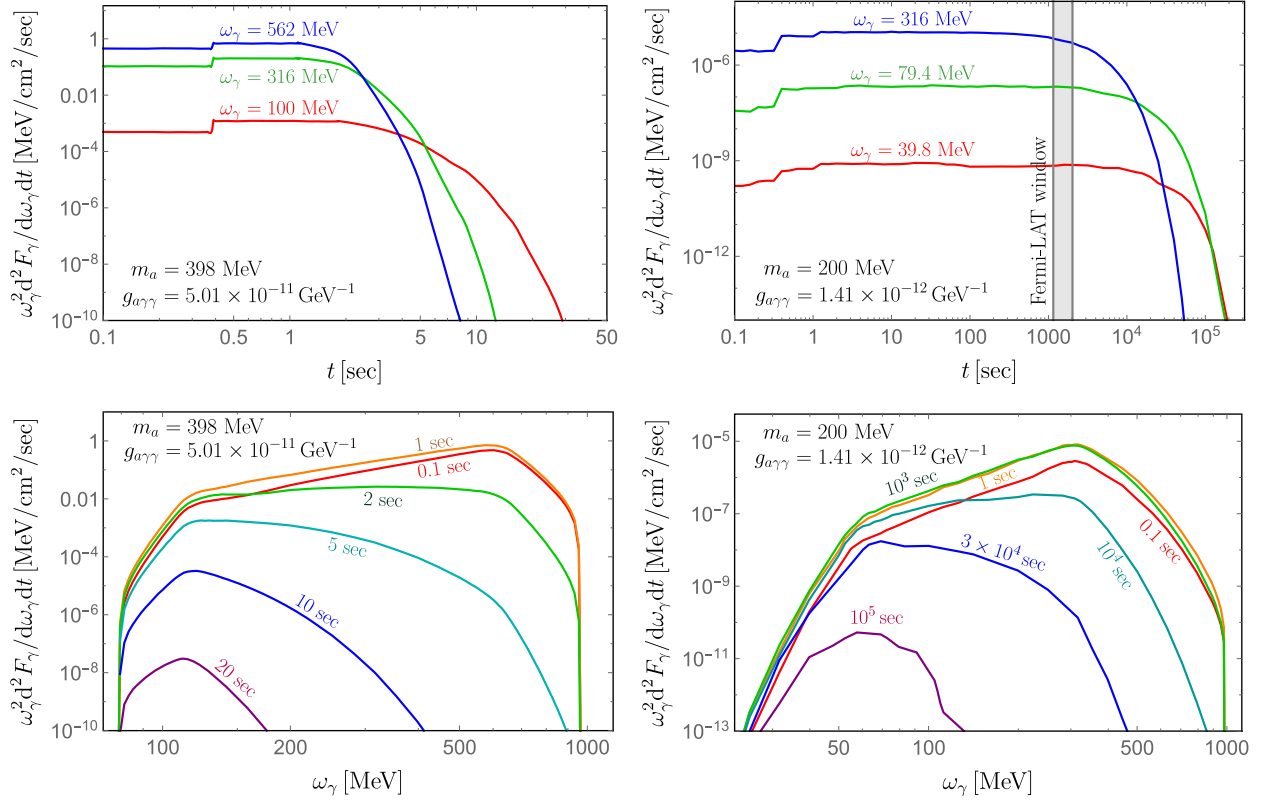

FIG. 3. Temporal (top) and spectral (bottom) behaviors of the photon flux coming from ALP decays. Left: correspond to benchmark 1 (shorter-lived ALPs with $m_a = 398$ MeV and $g_{a\gamma\gamma} = 5.01 \times 10^{-11}$ GeV^{-1}). Right: correspond to benchmark 2 (longer-lived ALPs with $m_a = 200$ MeV and $g_{a\gamma\gamma} = 1.41 \times 10^{-12}$ GeV^{-1}). The colored contours correspond to various spectral (top) and temporal (bottom) snapshots.

correlated photon-GW study of the merger is likely to be competitive. At such late times, the flux becomes softer and diminishes, with the spectral peak at $\omega_\gamma \sim 50$ MeV corresponding to $\omega_\gamma^2 d^2 F_\gamma / d\omega_\gamma dt \sim 10^{-10}$ MeV/cm^2/ sec (see the $t = 10^5$ sec curve in the bottom right panel); therefore, an instrument with peak sensitivity around $\omega_\gamma \sim 50$ MeV would be more effective there. (ii) For ALPs with shorter lifetimes corresponding to larger values of $g_{a\gamma\gamma}$ and/or m_a (benchmark 1), the photon flux reaches a temporal plateau and starts diminishing very early, around $t \sim \mathcal{O}(1)$ sec (see top left panel). For the time span $t \sim (0.1–1)$ sec, the spectral shape is broad between $\omega_\gamma \sim 100$ and 600 MeV, corresponding to $\omega_\gamma^2 d^2 F_\gamma / d\omega_\gamma dt \sim (0.1–1)$ MeV/cm^2/ sec (see bottom left panel). At later times $t \sim 10$ sec, the spectrum softens considerably, peaking at $\omega_\gamma \sim 120$ MeV, corresponding to $\omega_\gamma^2 d^2 F_\gamma / d\omega_\gamma dt \sim 10^{-5}$ MeV/cm^2/ sec.

From these benchmarks, two lessons for multimessenger studies of ALPs can be learned. First, timing and early coordination with the GW signal (within the first second) are most critical for short-lived ALPs, although the studies generally lose competitiveness for ALPs of all lifetimes beyond 10^5 sec. Interestingly, Fermi-LAT data from GW170817 [28] are just at this threshold. Second, instruments that are able to collect photon data early should have peak sensitivity in the hundreds of MeV; conversely, at late times, instruments with softer sensitivity in the tens of MeV are preferred.

Constraints.—We now turn to the constraints on the ALP mass versus coupling plane coming from multimessenger studies of GW170817. While a suite of x- and γ-ray instruments observed the event at different time slices, the data corresponding to Fermi-LAT observations [28] are the most optimal available data. Fermi-LAT was unable to obtain data from the prompt emission phase of the γ-ray burst associated with GW170817; the data collected corresponded to the time window (1153–2027) sec after the GW signal, in the (0.1–1) GeV energy range. The upper limit on the flux in this time and energy interval is 4.5×10^{-10} erg/cm^2/ sec [95% confidence level (CL)]. It should be noted that while the high-energy hard s-ray modulation telescope *Insight* was able to obtain data from much earlier times, its sensitivity range is (0.2–5) MeV [29], making it unsuitable for our purposes, as is evident from Fig. 3. Similarly, data from AGILE-GRID [(0.03–3) GeV, $t \sim 0.011$ days] [59], *Fermi* γ-ray burst monitor (Fermi-GBM) [(20–100) keV, $t \sim \pm 1$ days] [60], *INTEGRAL* IBIS/ISGRI [(20–300) keV, $t \sim (1–5.7)$ days] [27], *INTEGRAL* SPI [(300–4000) keV, $t \sim (1–5.7)$ days] [27], and H.E.S.S. [(0.27–3.27) TeV, $t \sim 1.22$ days] [61] yield weaker constraints due to a combination of spectral peak and timing, as do x-ray instruments like as do Swift-XRT [62], *Chandra* [63], and NuSTAR [62], which operate at even lower energies.
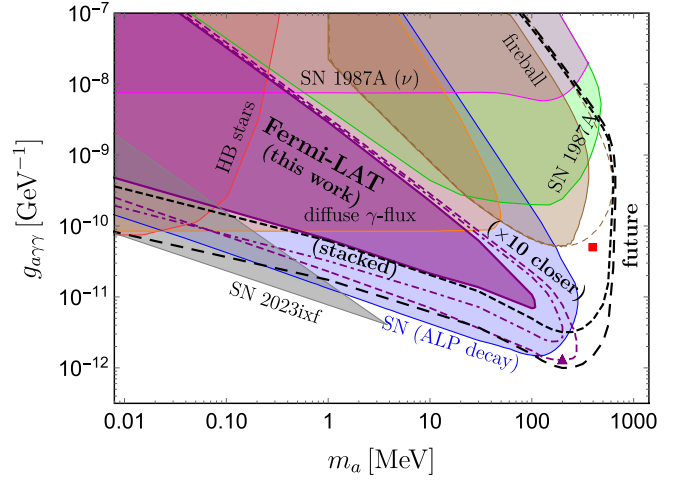

FIG. 4. Exclusion and sensitivity contours in the $(m_a, g_{a\gamma\gamma})$ plane; see text for details. The red square and purple triangle correspond, respectively, to benchmarks 1 and 2 in Fig. 3.

Figure 4 displays the main results of our study. The purple-shaded region is our 95% CL exclusion derived using Fermi-LAT data [28]. Here the merger remnant was assumed to survive for 1 sec, but varying this, and hence the ALP emission duration, between 0.72 and 1.29 sec (the range estimated by Ref. [55]) leads to very little change in the exclusion region. Furthermore, this constraint region depends little on the merger profile employed (see Fig. S3 [30]). Benchmark 1 (2) is shown with a red square (purple triangle) in Fig. 4. Some future projections are also displayed. The first projection, labeled as "(stacked)" (dot-dashed purple curve), corresponds to constraints coming from a stacked analysis of several mergers, all taken to be at $D = 40$ Mpc. The number of mergers in the stacked analysis depends on the predicted merger rate, which is $(10–1700)/\mathrm{Gpc}^3/\mathrm{yr}$ [64]. Within 40 Mpc, this rate predicts a merger every 2.2–370 yr; taking a mission lifetime of ~ 20 yr, we take the optimistic case of nine mergers in the stacked analysis. The second projection, labeled as "($\times 10$ closer)" (dashed purple curve), is for a single future merger that occurs at a distance 10 times closer to Earth ($D = 4$ Mpc), which is expected to happen every 2200–370 000 yr based on the same merger rate. A more likely projection is shown by the short-dashed black curve, obtained for the current Fermi-LAT flux upper limit [28], but with an early observation window of 0.1–100 sec. We also show a more futuristic projection (long-dashed black curve) for a hypothetical instrument with 100 times better flux sensitivity than the current Fermi-LAT limit and in a broader energy window of 1 MeV–1 GeV. This can happen, in principle, given the whole array of proposed MeV γ-ray missions, such as AMEGO-X [65], e-ASTROGAM [66], PANGU [67], AdEPT [68], APT [69], GAMMA-400 [70], and GECCO [71].

For comparison, the existing astrophysical constraints are also shown in Fig. 4, including those from horizontal branch (HB) star evolution (shaded red) [72], the diffuse γ-ray background from supernovae (shaded orange) [56], the SN1987A energy loss constraint from neutrino signal (shaded magenta) [56], calorimetric constraints from low-energy supernovae (shaded green) [56], and the SN1987A (shaded blue) [73,74] and SN2023ixf (shaded gray) [75] analogs of the γ-ray constraints. Also shown are the fireball formation (dashed brown) and exclusion (shaded brown) regions [76,77]. While the fireball region is taken directly from Ref. [77], and thus is based on different merger profiles than what we use here, the lower edge of the fireball region is almost independent of the merger profile (see Figs. 3 and S2 in Ref. [77]) and therefore is unlikely to affect our exclusion region or even the future sensitivity in the small $g_{a\gamma\gamma}$ region. There are additional cosmological constraints from cosmic microwave background and big bang nucleosynthesis on ALP coupling to photons [78,79], which are model dependent and hence not shown here.

Discussion and conclusions.—(i) This pertains to the relative utilities of mergers and supernovae in probing ALPs. If one ignores multimessenger and stacked analyses of mergers, supernovae enjoy an advantage that can be understood from the following considerations. Assuming that both merger and supernova emit equal ALP fluxes, and that the ALP decay length L (in the laboratory frame) is short compared to the distance D between the source and Earth, the photon flux from ALP decays F_γ goes as the probability that a given ALP has decayed by the time it reaches Earth, divided by D^2. Thus the ratio of F_γ^{SN} from a supernova at distance D_{SN} from the Earth and $F_\gamma^{\mathrm{merger}}$ from a merger at distance D_{merger} is $(D_{\mathrm{merger}}/D_{\mathrm{SN}})^2[1 - \exp(-D_{\mathrm{SN}}/L)]/[1 - \exp(-D_{\mathrm{merger}}/L)]$. Since $D_{\mathrm{SN,merger}} \gg L$, the above ratio is dominated by the quantity $(D_{\mathrm{merger}}/D_{\mathrm{SN}})^2$; therefore, a close-by supernova will provide a higher photon flux than a far-away merger. This is the main reason why our GW170817 constraint in Fig. 4 (purple shaded) is weaker than the SN1987A constraint (blue shaded).

However, after incorporating temporal information of the photon signal, the situation might change. Mergers offer a natural arena for such temporal multimessenger studies, since the time $t = 0$ can be defined relatively cleanly as the time of arrival of the GW signal. This is unlike the supernova case, where the timing uncertainty can be really large, especially if the neutrino signal is not detected, as, e.g., in the case of SN2023ixf [80]. As shown in Fig. 4, a combination of temporal-spectral merger data can be a powerful future probe of hitherto unconstrained parts of ALP parameter space.

(ii) It is important to emphasize that, since only flux upper limits from electromagnetic observations are used in our study, the conservative constraints derived here do not depend on the detailed modeling of the complex astrophysical background. However, the question of discriminating ALP-induced photons from astrophysical photons becomes very interesting in the early time window $t \sim (0–1)$ sec. Generally, photons emanating from BSM species like ALPs are expected to arrive before photons emanating from standard astrophysical processes. This is because BSM species couple feebly to material in the merger environment and escape promptly, thereafter decaying to photons in a more pristine environment away from the merger. As for the astrophysical MeV photon background from r-process nucleosynthesis [81–83], an analysis of panchromatic dataset from GW170817 [26] suggests a delayed x-ray and/or γ-ray signal with respect to the GW signal, consistent with the Fermi-GBM detection of the electromagnetic signal 1.7 sec after the GW detection [60]. Therefore, as shown by our temporal analysis, electromagnetic observations of the merger within the first second of the GW detection (possible with the early-warning system [84]) would be crucial to isolate the ALP-induced signal from astrophysical background. This is the subject of our upcoming work [85].

We also list here other possible follow-up studies. During a NS merger, the nuclear matter profiles change considerably over time [58,86], so ALP production should be calculated on top of these time-dependent profiles (as has been done for supernovae [87]) and ultimately included in the simulations themselves (also done in the case of supernovae for alternative ALP models [88,89]). Finally, the local ALP production rates can be refined by improving the treatment of the photon screening in dense matter [90] and by including other production channels like the electro-Primakoff effect [91,92].

*bdev@wustl.edu

†Jean-Francois.Fortin@phy.ulaval.ca

‡harrissp@uw.edu

§kuver.sinha@ou.edu

‖zhangyongchao@seu.edu.cn

[1] G. G. Raffelt, The astrophysics of neutrinos, axions, and other weakly interacting particles, in *Stars as Laboratories for Fundamental Physics* (1996).

[2] M. Baryakhtar *et al.*, Dark matter in extreme astrophysical environments, in *2022 Snowmass Summer Study* (2022), arXiv:2203.07984.

[3] J.-F. Fortin, H.-K. Guo, S. P. Harris, D. Kim, K. Sinha, and C. Sun, Axions: From magnetars and neutron star mergers to beam dumps and BECs, Int. J. Mod. Phys. D **30**, 2130002 (2021).

[4] B. P. Abbott *et al.* (LIGO Scientific and Virgo Collaborations), GW170817: Observation of gravitational waves from a binary neutron star inspiral, Phys. Rev. Lett. **119**, 161101 (2017).

[5] A. Hook and J. Huang, Probing axions with neutron star inspirals and other stellar processes, J. High Energy Phys. 06 (2018) 036.

[6] J. Huang, M. C. Johnson, L. Sagunski, M. Sakellariadou, and J. Zhang, Prospects for axion searches with Advanced LIGO through binary mergers, Phys. Rev. D **99**, 063013 (2019).

[7] T. Dietrich and K. Clough, Cooling binary neutron star remnants via nucleon-nucleon-axion bremsstrahlung, Phys. Rev. D **100**, 083005 (2019).

[8] S. P. Harris, J.-F. Fortin, K. Sinha, and M. G. Alford, Axions in neutron star mergers, J. Cosmol. Astropart. Phys. 07 (2020) 023.

[9] J. Zhang, Z. Lyu, J. Huang, M. C. Johnson, L. Sagunski, M. Sakellariadou, and H. Yang, First constraints on nuclear coupling of axionlike particles from the binary neutron star gravitational wave event GW170817, Phys. Rev. Lett. **127**, 161101 (2021).

[10] D. F. G. Fiorillo and F. Iocco, Axions from neutron star mergers, Phys. Rev. D **105**, 123007 (2022).

[11] T. K. Poddar, A. Ghoshal, and G. Lambiase, Listening to dark sirens from gravitational waves: Combined effects of fifth force, ultralight particle radiation, and eccentricity, arXiv:2302.14513.

[12] P. S. B. Dev, J.-F. Fortin, S. P. Harris, K. Sinha, and Y. Zhang, Light scalars in neutron star mergers, J. Cosmol. Astropart. Phys. 01 (2022) 006.

[13] M. D. Diamond and G. Marques-Tavares, γ-ray flashes from dark photons in neutron star mergers, Phys. Rev. Lett. **128**, 211101 (2022).

[14] B. P. Abbott *et al.* (LIGO Scientific, Virgo, Fermi-GBM, and INTEGRAL Collaborations), Gravitational waves and gamma-rays from a binary neutron star merger: GW170817 and GRB 170817A, Astrophys. J. Lett. **848**, L13 (2017).

[15] B. P. Abbott *et al.*, Multi-messenger observations of a binary neutron star merger, Astrophys. J. Lett. **848**, L12 (2017).

[16] S. Weinberg, A new light boson?, Phys. Rev. Lett. **40**, 223 (1978).

[17] F. Wilczek, Problem of strong p and t invariance in the presence of instantons, Phys. Rev. Lett. **40**, 279 (1978).

[18] J. E. Kim, Weak interaction singlet and strong CP invariance, Phys. Rev. Lett. **43**, 103 (1979).

[19] M. A. Shifman, A. I. Vainshtein, and V. I. Zakharov, Can confinement ensure natural CP invariance of strong interactions?, Nucl. Phys. **B166**, 493 (1980).

[20] A. R. Zhitnitsky, On possible suppression of the axion hadron interactions (in Russian), Sov. J. Nucl. Phys. **31**, 260 (1980).

[21] M. Dine, W. Fischler, and M. Srednicki, A simple solution to the strong CP problem with a harmless axion, Phys. Lett. **104B**, 199 (1981).

[22] P. Svrcek and E. Witten, Axions in string theory, J. High Energy Phys. 06 (2006) 051.

[23] M. Reece, TASI lectures: (No) global symmetries to axion physics, Proc. Sci., TASI2022 (**2024**) 008 [arXiv:2304.08512].

[24] I. G. Irastorza and J. Redondo, New experimental approaches in the search for axion-like particles, Prog. Part. Nucl. Phys. **102**, 89 (2018).

[25] P. Sikivie, Invisible axion search methods, Rev. Mod. Phys. **93**, 015004 (2021).

[26] M. M. Kasliwal *et al.*, Illuminating gravitational waves: A concordant picture of photons from a neutron star merger, Science **358**, 1559 (2017).

[27] V. Savchenko *et al.*, INTEGRAL detection of the first prompt gamma-ray signal coincident with the gravitational-wave event GW170817, Astrophys. J. Lett. **848**, L15 (2017).

[28] M. Ajello *et al.*, Fermi-LAT observations of LIGO/Virgo event GW170817, Astrophys. J. **861**, 85 (2018).

[29] T. Li *et al.* (Insight-HXMT Team Collaboration), Insight-HXMT observations of the first binary neutron star merger GW170817, Sci. China Phys. Mech. Astron. **61**, 031011 (2018).

[30] See Supplemental Material at http://link.aps.org/supplemental/10.1103/PhysRevLett.132.101003 for the details of ALP production, NS merger profiles, and ALP decay geometry, which includes Refs. [31–53].

[31] E. Braaten and D. Segel, Neutrino energy loss from the plasma process at all temperatures and densities, Phys. Rev. D **48**, 1478 (1993).

[32] J. B. Adams, M. A. Ruderman, and C. H. Woo, Neutrino pair emission by a stellar plasma, Phys. Rev. **129**, 1383 (1963).

[33] G. G. Raffelt, Comment on axion emission rates in stars, Phys. Rev. D **34**, 3927 (1986).

[34] G. G. Raffelt and D. S. P. Dearborn, Bounds on hadronic axions from stellar evolution, Phys. Rev. D **36**, 2211 (1987).

[35] G. Lucente, P. Carenza, T. Fischer, M. Giannotti, and A. Mirizzi, Heavy axion-like particles and core-collapse supernovae: Constraints and impact on the explosion mechanism, J. Cosmol. Astropart. Phys. 12 (2020) 008.

[36] A. Caputo, A. J. Millar, and E. Vitagliano, Revisiting longitudinal plasmon-axion conversion in external magnetic fields, Phys. Rev. D **101**, 123004 (2020).

[37] P. Carenza, O. Straniero, B. Döbrich, M. Giannotti, G. Lucente, and A. Mirizzi, Constraints on the coupling with photons of heavy axion-like-particles from globular clusters, Phys. Lett. B **809**, 135709 (2020).

[38] M. Bastero-Gil, C. Beaufort, and D. Santos, Solar axions in large extra dimensions, J. Cosmol. Astropart. Phys. 10 (2021) 048.

[39] R. Z. Ferreira, M. C. D. Marsh, and E. Müller, Strong supernovae bounds on ALPs from quantum loops, J. Cosmol. Astropart. Phys. 11 (2022) 057.

[40] M. G. Alford, A. Haber, S. P. Harris, and Z. Zhang, Beta equilibrium under neutron star merger conditions, Universe **7**, 399 (2021).

[41] M. G. Alford and S. P. Harris, Beta equilibrium in neutron star mergers, Phys. Rev. C **98**, 065806 (2018).

[42] G. Camelio, T. Dietrich, M. Marques, and S. Rosswog, Rotating neutron stars with nonbarotropic thermal profile, Phys. Rev. D **100**, 123001 (2019).

[43] W. Kastaun, R. Ciolfi, and B. Giacomazzo, Structure of stable binary neutron star merger remnants: A case study, Phys. Rev. D **94**, 044060 (2016).

[44] M. Hanauske, J. Steinheimer, A. Motornenko, V. Vovchenko, L. Bovard, E. R. Most, L. J. Papenfort, S. Schramm, and H. Stöcker, Neutron star mergers: Probing the EoS of hot, dense matter by gravitational waves, Particles **2**, 44 (2019).

[45] M. Hanauske, K. Takami, L. Bovard, L. Rezzolla, J. A. Font, F. Galeazzi, and H. Stocker, Rotational properties of hypermassive neutron stars from binary mergers, Phys. Rev. D **96**, 043004 (2017).

[46] A. Caputo, G. Raffelt, and E. Vitagliano, Muonic boson limits: Supernova redux, Phys. Rev. D **105**, 035022 (2022).

[47] A. Sung, G. Guo, and M.-R. Wu, Supernova constraint on self-interacting dark sector particles, Phys. Rev. D **103**, 103005 (2021).

[48] N. K. Glendenning, *Compact Stars: Nuclear Physics, Particle Physics, and General Relativity* (Springer, New York, 1997).

[49] K. Engel et al., The future of gamma-ray experiments in the MeV-EeV range, in *Proceedings of the Snowmass 2021* (2022), arXiv:2203.07360.

[50] G. Camelio, T. Dietrich, S. Rosswog, and B. Haskell, Axisymmetric models for neutron star merger remnants with realistic thermal and rotational profiles, Phys. Rev. D **103**, 063014 (2021).

[51] G. Camelio, T. Dietrich, S. Rosswog, and B. Haskell, Axisymmetric models for neutron star merger remnants with realistic thermal and rotational profiles: Dataset (2020), 10.5281/zenodo.4268500.

[52] M. Alford, M. Braby, M. W. Paris, and S. Reddy, Hybrid stars that masquerade as neutron stars, Astrophys. J. **629**, 969 (2005).

[53] J. S. Read, B. D. Lackey, B. J. Owen, and J. L. Friedman, Constraints on a phenomenologically parameterized neutron-star equation of state, Phys. Rev. D **79**, 124032 (2009).

[54] S. Bernuzzi, Neutron star merger remnants, Gen. Relativ. Gravit. **52**, 108 (2020).

[55] R. Gill, A. Nathanail, and L. Rezzolla, When did the remnant of GW170817 collapse to a black hole?, Astrophys. J. **876**, 139 (2019).

[56] A. Caputo, H.-T. Janka, G. Raffelt, and E. Vitagliano, Low-energy supernovae severely constrain radiative particle decays, Phys. Rev. Lett. **128**, 221103 (2022).

[57] P. Arras and N. N. Weinberg, Urca reactions during neutron star inspiral, Mon. Not. R. Astron. Soc. **486**, 1424 (2019).

[58] A. Perego, S. Bernuzzi, and D. Radice, Thermodynamics conditions of matter in neutron star mergers, Eur. Phys. J. A **55**, 124 (2019).

[59] F. Verrecchia et al., AGILE observations of the gravitational-wave source GW170817: Constraining gamma-ray emission from a NS-NS coalescence, Astrophys. J. Lett. **850**, L27 (2017).

[60] A. Goldstein et al., An ordinary short gamma-ray burst with extraordinary implications: Fermi-GBM detection of GRB 170817A, Astrophys. J. Lett. **848**, L14 (2017).

[61] H. Abdalla et al. (H.E.S.S. Collaboration), TeV gamma-ray observations of the binary neutron star merger GW170817 with H.E.S.S, Astrophys. J. Lett. **850**, L22 (2017).

[62] P. Evans, J. A. Kennea, A. A. Breeveld et al., GCN, 21550, 2017, https://ui.adsabs.harvard.edu/abs/2017GCN.21550... .1E.

[63] R. Margutti, W. Fong, E. Berger et al., GCN, 21648, 2017, https://ui.adsabs.harvard.edu/abs/2017GCN.21648....1M.

[64] R. Abbott et al. (KAGRA, VIRGO, and LIGO Scientific Collaborations), Population of merging compact binaries inferred using gravitational waves through GWTC-3, Phys. Rev. X **13**, 011048 (2023).

[65] R. Caputo et al., All-sky medium energy gamma-ray observatory explorer mission concept, J. Astron. Telesc. Instrum. Syst. **8**, 044003 (2022).

[66] A. De Angelis et al. (e-ASTROGAM), Science with e-ASTROGAM: A space mission for MeV–GeV gamma-ray astrophysics, J. High Energy Astrophysics **19**, 1 (2018).

[67] X. Wu, M. Su, A. Bravar, J. Chang, Y. Fan, M. Pohl et al., PANGU: A high resolution gamma-ray space telescope, Proc. SPIE Int. Soc. Opt. Eng. **9144**, 91440F (2014).

[68] S. D. Hunter et al., A pair production telescope for medium-energy gamma-ray polarimetry, Astropart. Phys. **59**, 18 (2014).

[69] J. H. Buckley et al. (APT Collaboration), The advanced particle-astrophysics telescope (APT) project status, Proc. Sci., ICRC20212021 (**2021**) 655.

[70] A. M. Galper et al., Precision measurements of high-energy cosmic gamma-ray emission with the GAMMA-400 gamma-ray telescope, Phys. At. Nucl. **80**, 1141 (2017).

[71] E. Orlando et al., Exploring the MeV sky with a combined coded mask and Compton telescope: The Galactic Explorer with a coded aperture mask Compton telescope (GECCO), J. Cosmol. Astropart. Phys. 07 (2022) 036.

[72] G. Lucente, O. Straniero, P. Carenza, M. Giannotti, and A. Mirizzi, Constraining heavy axionlike particles by energy deposition in globular cluster stars, Phys. Rev. Lett. **129**, 011101 (2022).

[73] E. Müller, F. Calore, P. Carenza, C. Eckner, and M. C. D. Marsh, Investigating the gamma-ray burst from decaying MeV-scale axion-like particles produced in supernova explosions, J. Cosmol. Astropart. Phys. 07 (2023) 056.

[74] S. Hoof and L. Schulz, Updated constraints on axion-like particles from temporal information in supernova SN1987A gamma-ray data, J. Cosmol. Astropart. Phys. 03 (2023) 054.

[75] E. Müller, P. Carenza, C. Eckner, and A. Goobar, Constraining MeV-scale axionlike particles with Fermi-LAT observations of SN 2023ixf, Phys. Rev. D **109**, 023018 (2024).

[76] M. Diamond, D. F. G. Fiorillo, G. Marques-Tavares, and E. Vitagliano, Axion-sourced fireballs from supernovae, Phys. Rev. D **107**, 103029 (2023).

[77] M. Diamond, D. Fiorillo, G. Marques-Tavares, I. Tamborra, and E. Vitagliano, following Letter, Multimessenger constraints on radiatively decaying axions from GW170817, Phys. Rev. Lett. **132**, 101004 (2024).

[78] P. F. Depta, M. Hufnagel, and K. Schmidt-Hoberg, Robust cosmological constraints on axion-like particles, J. Cosmol. Astropart. Phys. 05 (2020) 009.

[79] C. Balázs *et al.*, Cosmological constraints on decaying axion-like particles: A global analysis, J. Cosmol. Astropart. Phys. 12 (2022) 027.

[80] J. Thwaites *et al.*, The Astronomer's Telegram, 16043 (2023), https://ui.adsabs.harvard.edu/abs/2023ATel16043....1T.

[81] J. M. Lattimer and D. N. Schramm, Black-hole-neutron-star collisions, Astrophys. J. Lett. **192**, L145 (1974).

[82] D. Eichler, M. Livio, T. Piran, and D. N. Schramm, Nucleosynthesis, neutrino bursts and gamma-rays from coalescing neutron stars, Nature (London) **340**, 126 (1989).

[83] S. Rosswog, C. Freiburghaus, and F. K. Thielemann, Nucleosynthesis calculations for the ejecta of neutron star coalescences, Nucl. Phys. **A688**, 344 (2001).

[84] S. Sachdev *et al.*, An early-warning system for electromagnetic follow-up of gravitational-wave events, Astrophys. J. Lett. **905**, L25 (2020).

[85] P. S. B. Dev, J.-F. Fortin, S. P. Harris, K. Sinha, and Y. Zhang, New physics in the first second after neutron star mergers (to be published).

[86] M. G. Alford, L. Bovard, M. Hanauske, L. Rezzolla, and K. Schwenzer, Viscous dissipation and heat conduction in binary neutron-star mergers, Phys. Rev. Lett. **120**, 041101 (2018).

[87] A. Payez, C. Evoli, T. Fischer, M. Giannotti, A. Mirizzi, and A. Ringwald, Revisiting the SN1987A gamma-ray limit on ultralight axion-like particles, J. Cosmol. Astropart. Phys. 02 (2015) 006.

[88] T. Fischer, P. Carenza, B. Fore, M. Giannotti, A. Mirizzi, and S. Reddy, Observable signatures of enhanced axion emission from protoneutron stars, Phys. Rev. D **104**, 103012 (2021).

[89] T. Fischer, S. Chakraborty, M. Giannotti, A. Mirizzi, A. Payez, and A. Ringwald, Probing axions with the neutrino signal from the next galactic supernova, Phys. Rev. D **94**, 085012 (2016).

[90] S. Stetina, E. Rrapaj, and S. Reddy, Photons in dense nuclear matter: Random-phase approximation, Phys. Rev. C **97**, 045801 (2018).

[91] C. Dessert, A. J. Long, and B. R. Safdi, No evidence for axions from Chandra observation of the magnetic white dwarf RE J0317-853, Phys. Rev. Lett. **128**, 071102 (2022).

[92] T. Altherr and U. Kraemmer, Gauge field theory methods for ultradegenerate and ultrarelativistic plasmas, Astropart. Phys. **1**, 133 (1992).